RSC Advances

PAPER

View Article Online
View Journal | View Issue



Cite this: *RSC Adv.*, 2018, **8**, 27008

# A novel biosensor based on ball-flower-like Cu-hemin MOF grown on elastic carbon foam for trichlorfon detection†

Yonggui Song, Baixi Shan, Bingwei Feng, Pengfei Xu, Qiang Zeng and Dan Su *

In this study, ball-flower-like Cu-hemin MOFs microstructures supported by flexible three-dimensional (3D) nitrogen-containing melamine carbon foam composites (denoted as Cu-H MOFs/NECF) were constructed. They were used for the immobilization of acetylcholinesterase (AChE) to detect trichlorfon, a widely applicable organophosphorus pesticide (OP). The formation of Cu-H MOFs/NECF was confirmed by scanning electron microscopy, X-ray powder diffraction and energy-dispersive X-ray spectroscopy. The results indicated that ball-flower-like Cu-hemin MOF microstructures were evenly grown on the fibers of 3D-NECF *via* a simple room temperature mixing method, which could greatly increase the effective surface area. The Cu-H MOFs/NECF composites also overcome the disadvantages of carbon foam materials such as too large pore diameters that always lead to the stacking of the protease and poor conductivity. Moreover, the composites contain nitrogen elements not only from melamine but also from hemin, which is bound to greatly increase the biocompatibility. The composites were directly used to immobilize a large number of AChE to prepare integrated AChE/Cu-H MOFs/NECF electrodes. Simultaneously, the integrated electrode showed better performance for trichlorfon detection. The sensor exhibited good stability and toughness, wide linear range (0.25–20 ng $mL^{-1}$) and low detection limit (0.082 ng $mL^{-1}$). Hence, the AChE/Cu-H MOFs/NECF trichlorfon sensor could be a valuable platform for the pesticide residues field testing.

Received 29th May 2018
Accepted 15th July 2018

DOI: 10.1039/c8ra04596h

rsc.li/rsc-advances



## 1. Introduction

Trichlorfon, one of the organophosphorus pesticides (OPs), has been extensively used in agriculture owing to its high insecticidal activity.[1,2] However, it presents a serious risk to human health due to its inhibitory effect on acetylcholinesterase (AChE),[3–5] a key enzyme for the nerve transmission. Thus, a fast and sensitive detection of pesticide residues in food has become increasingly important. Traditional analytical methods, such as gas chromatography[6,7] or high-performance liquid chromatography,[8,9] often coupled with mass-selective detectors, are significantly time-consuming and expensive. These methods are still performed in laboratory, but they are not suitable for fast field detection. Consequently, the development of rapid and sensitive OP detecting techniques with low detection limits has increasing potential for environmental monitoring and food industry.

Amperometric AChE biosensors[10–13] present a promising alternative method to the traditional strategies because of their high sensitivity, fast response, and miniature size. Based on the inhibitory action of OPs on AChE, the concentrations of pesticides could be precisely determined. The sensitivity and the detection limit of these biosensors depend on the number of enzyme molecules,[14,15] and thus, immobilization of the enzyme on the surface of electrodes is a crucial step for the performance of the biosensors. In order to firmly immobilize the enzyme, numerous advanced materials such as carbon nanotubes,[16–19] gold nanoparticles,[20–22] and porous materials[23,24] have been introduced for the construction of enzyme-loaded matrixes. The integration of enzyme and porous materials greatly promoted the sensitivity, stability and detection limit of enzyme biosensors. However, lack of flexibility is still a drawback of such materials. In our group, an elastic nitrogen-containing carbon foam was prepared as an integrated electrode by carbonization of a cheap heat-insulating material-melamine foam.[25] This carbon foam has three-dimensional network structure, large surface area and robust character. We directly modified the glucose oxidase on this carbon foam and achieved good results for glucose sensing. However, at the same time, it was found that the apertures of the carbon foam are too large (about 25 μm), which led to a series of drawbacks such as the protein stacking, which may affect the enzyme's function and reduce its conductivity.[26]

In this study, the Cu-hemin MOF microstructures supported by flexible three-dimensional (3D) nitrogen-containing melamine carbon foam (denoted as Cu-H MOFs/NECF) composites were constructed *via* using a simple one-step method. The Cu-hemin MOFs could firmly grow on the fibres of porous NECF.

*Jiangxi University of Traditional Chinese Medicine, 1688 Meiling Road, Nanchang 330006, China. E-mail: sud94@aliyun.com; Fax: +86 791 87802135; Tel: +86 791 87802135*

† Electronic supplementary information (ESI) available. See DOI: 10.1039/c8ra04596h

In addition, the Cu-hemin MOFs had good biocompatibility because they were fabricated *via* $Cu^{2+}$ coordination with hemin and thus, it contained abundant nitrogen that came from hemin. The Cu-hemin MOFs also showed a 3D ball-flower-like nanostructure, which overlapped with the network structure of NECF, and could be used to load a large number of AChE molecules. The AChE molecules were incorporated into Cu-hemin MOFs by utilizing the associated pores of MOFs, which effectively avoided the aggregation of enzyme molecules on the surface of the electrode. The ball-flower-like nanostructure of Cu-hemin MOFs resulted in the contact of AChE molecules with OP and electrolyte to ensure that the enzyme inhibition reaction was fully carried out. Moreover, the metal sites of Cu-hemin MOFs could increase the conductivity of the integrated electrode. The as-prepared trichlorfon sensor based on the AChE/Cu-hemin MOF/NECF composites exhibited a wide linear range, low detection limit and good toughness.

# 2. Experimental

## 2.1 Reagents and materials

MFs were obtained from SINOYQX (Sichuan, China) and used as received. Acetylcholinesterase (1000 U $mg^{-1}$) and acetylthiocholine chloride (ATCl) were purchased from Sigma-Aldrich (St Louis, USA). Trichlorfon was purchased from Lanxi pesticide factory. Other reagents were of analytical reagent grade and purchased from Beijing Chemical Reagent Factory (Beijing, China). All solutions were prepared using ultrapure water purified by a Millipore-Q System (18.2 MΩ cm). The solutions were deoxygenated by nitrogen before experiments. Phosphate buffer solution (PBS) was prepared from sodium dihydrogen phosphate and disodium hydrogen phosphate.

## 2.2 Preparation of AChE/Cu-hemin MOFs/NECFE

The NECF was prepared by carbonization of MF in a high-temperature furnace according to the previous study.[25] The MFs were placed in an electric furnace, heated to a certain temperature (900 °C) at a heating rate of 5 °C $min^{-1}$ under nitrogen atmosphere and annealed for about 0.5 h at 900 °C to finish the carbonization process. The as-prepared ECFs were taken out after the temperature was cooled down to below 200 °C. Then, the NECF was cut into a cylindrical shape with the outside diameter almost equal to the inside diameter of the treated pipette tip. The processed NECF was washed with ethanol and ultra-pure water, in sequence, and dried naturally to be ready for use. Cu-hemin MOFs/NECFs were synthesized according to the following procedure. 43 mM $Cu(NO_3)_2 \cdot 3H_2O$ and 0.50 mM hemin (in PBS solution, pH = 7) were mixed in a volume ratio of 2 : 1 and then, the as-prepared NECFs were added into the mixed solution and stirred for 2 h at 25 °C. Following this, the Cu-hemin MOFs/NECFs were taken out and washed with ultrapure water 5 times and then dried in a vacuum oven at 40 °C for 24 h. Subsequently, the Cu-hemin MOFs/NECFs were inserted into the treated pipette tip. Then, 1.0 g graphite powder and 0.25 g liquid paraffin were mixed and homogenized carefully in an agate mortar for 20 min. Following this, the homogenized mixture was packed into the upper part of the pipette tip to contact the end of NECF. Then, a copper wire was inserted into the pipette tip to electrically connect the tip with the end of NECF *via* graphite powder. After the homogenized mixture paste was naturally dried at room temperature, the copper wire was further immobilized by using parafilm or epikote, as shown in Fig. S1 (ESI†). The AChE/Cu-hemin MOFs/NECF electrode was prepared by coating 5.0 μL AChE solution of different concentrations onto the electrode surface and then, the electrode was dried. The entire preparation process is shown in Fig. S1 (ESI†) and Scheme 1. Finally, the modified electrode was rinsed with ultrapure water to remove those weakly bound substances and stored at 4 °C for further use. The resulting AChE/Cu-hemin MOFs/NECF electrode was referred to as AChE/Cu-H MOFs/NECFE.

## 2.3 Apparatus

Cyclic voltammograms (CVs) and differential pulse voltammetries (DPVs) were carried out using a CHI760E electrochemical workstation (Shanghai, China). A three-electrode configuration was used with a platinum wire as the auxiliary electrode, a saturated calomel electrode (SCE) as the reference electrode, and an AChE/Cu-hemin MOF/NECF as the working electrode. CVs and DPVs were carried out in 10.0 mL of 0.2 M PBS (pH 7.0) at room temperature. Scanning electron microscopy (SEM) analysis was performed using an XL30 ESEM-FEG SEM equipped with a Phoenix energy dispersive X-ray analyzer (EDXA) at an accelerating voltage of 20 kV.

## 2.4 Inhibition measurement using AChE biosensor

A detailed description of the assay process for trichlorfon is illustrated in Fig. 1. For inhibition tests, the original differential pulse voltammetric signal ($I_{P,control}$) was measured in 0.1 M pH 7.0 PBS with 1.0 mM ATCl. Then, the electrode was rinsed with water and incubated in an aqueous solution containing the desired concentration of trichlorfon for 10 min. After incubation, the residual signal ($I_{P,exp}$) was recorded under the same condition. The inhibition rate of trichlorfon was calculated as follows:

$$\text{Inhibition } (\%) = 100\% \times \frac{I_{P,control} - I_{P,exp}}{I_{P,exp}}$$

# 3. Results and discussion

## 3.1 Characterization of AChE/Cu-H MOFs/NECFE

Unlike the reticulated vitreous carbon, which showed a brittle characteristic, the NECF was elastic and could sustain a large-strain compressing or bending deformation, and recovered most of its volume elastically, as shown in Fig. 1A, indicating that the as-prepared NECF inherited the superelastic characteristics of the precursor MF. The SEM image in Fig. 1B revealed that the as-prepared NECF possesses the interconnected network architecture and neuronal axon-like fibers. The architecture was similar to that of crosslinked nerve cells, which

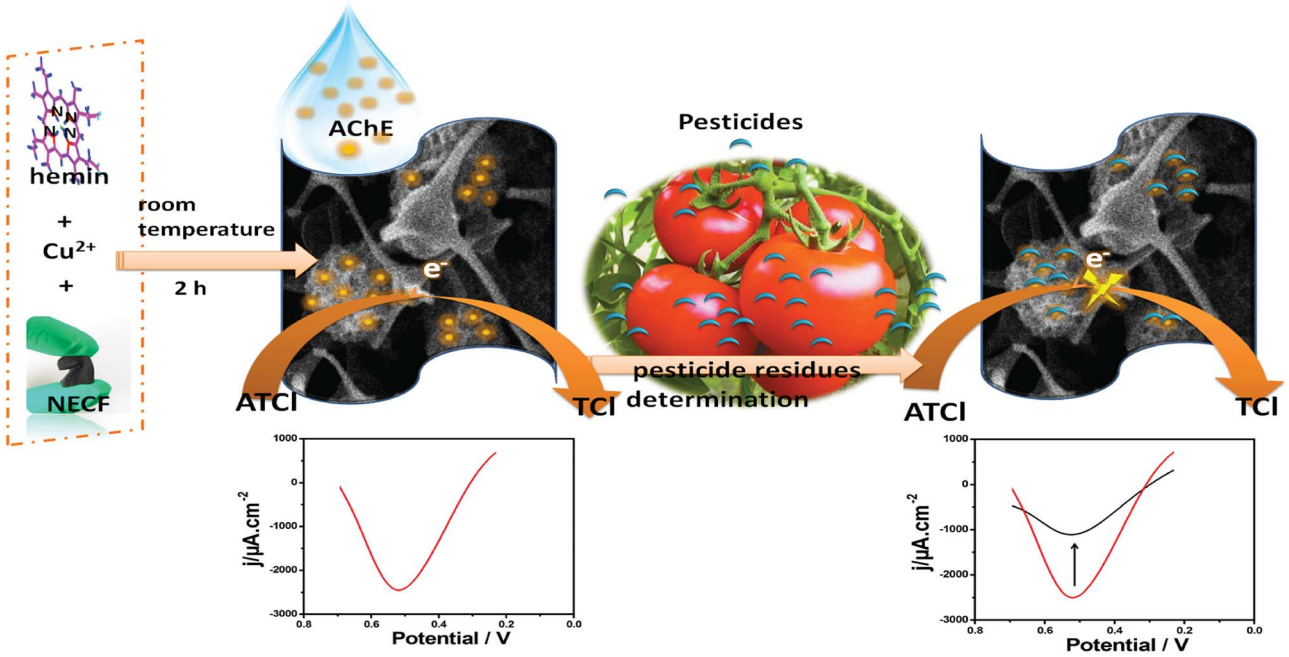


Scheme 1 Schematic of the AChE/Cu-hemin MOFs/NECF electrochemical pesticides biosensor.

could greatly increase the electrical conductivity and specific surface area of NECF. Moreover, the neuronal axon-like fibers were beneficial for the adsorption of enzyme.[25] As shown in Fig. 1C, a large number of uniform 3D Cu-hemin MOFs with ball-flower-like structures grew firmly on the netlike carbon foam. Moreover, it could also be seen from Fig. 1D and S2AB (ESI†) that the Cu-hemin MOFs showed a large number of holes in the flower-like ball, which could not only provide a large specific surface area but also enhance the mass transfer. The special structure of hemin might result in the formation of such ball-flower-like structure *via* a linkage between $Cu^{2+}$ and carboxy groups of hemin. As a fixed-structure molecule, hemin owned three characteristic elements (Fe, N and Cl) combined with the inherent elements (C and N) of melamine carbon foam,[25] which could be used to prove its existence.[27–29] As could be seen from energy-dispersive X-ray spectra in Fig. 1E, the apparent peaks of Fe, N, Cl and Cu were observed in the solid products, which declared the formation of Cu-hemin MOFs. In order to verify this conclusion, the X-ray powder diffraction (XRD) test were carried out, and the XRD spectra of Cu-hemin MOFs are exhibited in Fig. 1F. Some diffraction peaks appeared in the pattern of Cu-hemin MOFs, suggesting that the 3D-flower-like ball nanostructure was a crystalline material and the crystal structure of Cu-hemin MOFs was similar to that of previous hemin-MOFs.[30,31] All the results confirmed that the 3D-flower-like ball nanostructures were ascribed to the Cu-hemin MOFs with ordered structure and high crystallinity.

### 3.2 Cyclic voltammetry behavior of biosensor

Fig. 2A shows the cyclic voltammograms (CVs) of different electrodes in PBS containing 1.0 mM ATCl at pH 7.0. The CV of the AChE/Cu-H MOFs/NECFE showed an irreversible oxidation peak at 670 mV (curve a), which was attributed to the oxidation of thiocholine, a hydrolysis product of ATCl, catalyzed by the enzyme. In contrast, the peak current of AChE/NECFE without the growth of Cu-H MOFs (curve b) and AChE/carbon paste electrode (AChE/CPE) (curve c) was much lower. The increase of the response may induced by the synergistic effect of Cu-H MOFs and NECFs, which had large surface area that could immobilize more amounts of enzymes, and also due to the advantage of fast electron transfer of Cu-H MOFs owing to the metal loci and ball-flower-shaped structure. Moreover, the good biocompatibility of Cu-H MOFs/NECF could well maintain the maximum bioactivity of the immobilized enzyme. After the AChE/Cu-H MOFs/NECFE was incubated in 10 ng $mL^{-1}$ and 20 ng $mL^{-1}$ trichlorfon solution for 10 min, the anodic peak currents (curves b and c, Fig. 2B) drastically decreased compared with those of the control (curve a, Fig. 2B); this decreasing trend increased with the increase in concentration of trichlorfon. This was because trichlorfon, as an OP compound, exhibited acute toxicity and was involved in the irreversible inhibitory action on AChE, thus reducing the enzymatic activity on its substrate. Based on the change in voltammetric signal of the AChE/Cu-H MOFs/NECFE, the trichlorfon concentration could be detected. The detection principle is shown in Scheme 1.

### 3.3 Influence of ATCl, AChE concentration and pH value

Fig. 3A shows the amperometric response of AChE/Cu-H MOFs/NECFE to the addition of ATCl. The typical current–time response curve of the biosensor was obtained by successive additions of the substrate into a stirred cell. With the increase in concentration of ATCl, the amperometric response increased, and got to a plateau at 1.0 mM. The reason for this phenomenon

 

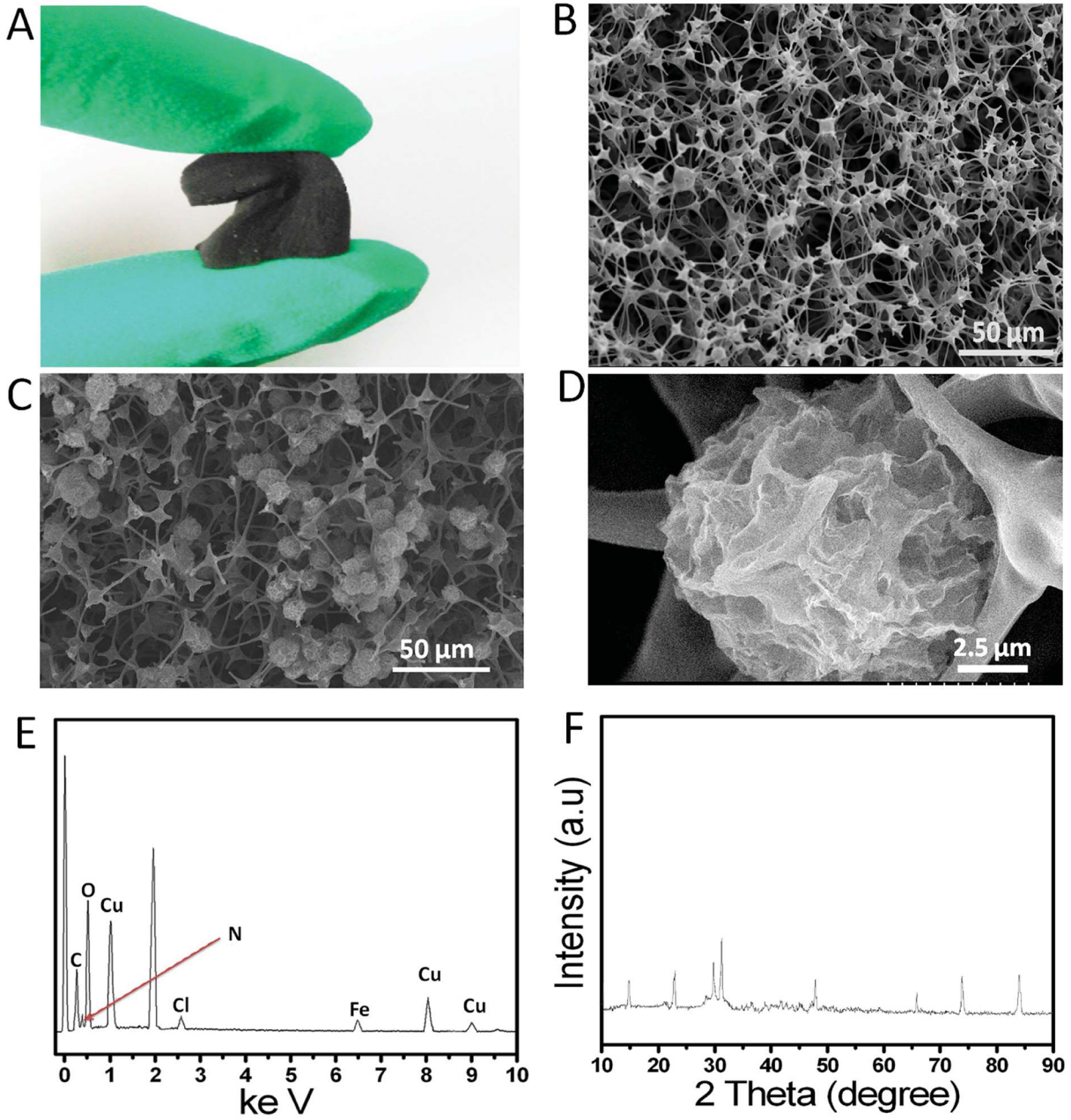


Fig. 1 (A) Melamine foam bent by finger tips. (B) SEM images of NECF. (C) SEM images of Cu-hemin MOFs/NECF. (D) The magnified image of one Cu-hemin MOF in the NECF. (E) EDS curve of Cu-hemin MOFs. (F) XRD patterns of Cu-hemin MOFs.

was that the increase in ATCl concentration caused a saturation of the active sites on enzyme by ATCl, leaving fewer sites available for new molecules to bind. Consequently, the rate of increase in peak current showed a decrement. Therefore, 1.0 mM ATCl was chosen as the uniform concentration in the following experiments for the pesticide analysis.

The amount of AChE immobilized on the electrode surface was another important factor related to the performance of the biosensor. Fig. 3B displays the plot of AChE concentration *versus* the amperometric response of the biosensor. With the increase in AChE concentration, the peak current increased gradually and reached the maximum value at 25 U $mL^{-1}$. Following this, the amperometric response decreased gradually as the concentration of AChE further increased. These behaviors might be attributed to the fact that the too few AChE molecules would not be sufficient for catalytic oxidation of glucose and the too thick modified layer of AChE might hinder both the electron and the mass transfer to decrease the catalytic current. This issue might be ascribed to the fact that a large number of AChE would block the approaching Cu-H MOFs/NECF (to produce thiocholine) and electron transfer. Thus, 25 U $mL^{-1}$ AChE solution was used to construct AChE/Cu-H MOFs/NECFE in the following experiments.

For the electrochemical biosensors, the pH value was a crucial factor influencing the sensitivity and stability. Therefore, the effect of pH was further investigated. As shown in

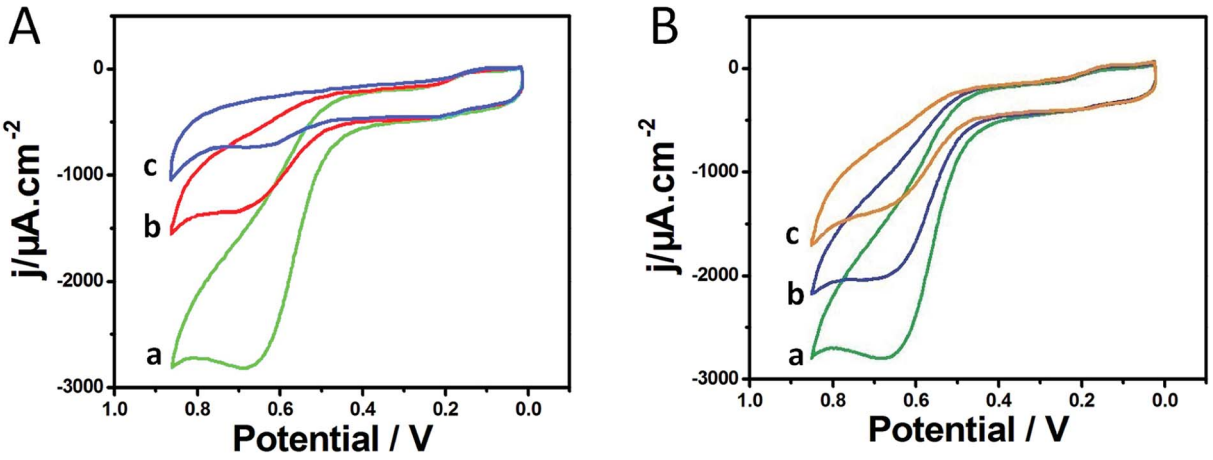


Fig. 2 (A) CVs of the AChE/Cu-H MOFs/NECFE (a), AChE/NECFE (b) and AChE/CPE (c) in 0.1 M PBS 7.0 solution containing 1.0 mM ATCl, and (B) CVs of AChE/Cu-H MOFs/NECFE in PBS 7.0 solution before (a) and after the inhibition by 10 ng $mL^{-1}$ (b) and 20 ng $mL^{-1}$ (c) trichlorfon.

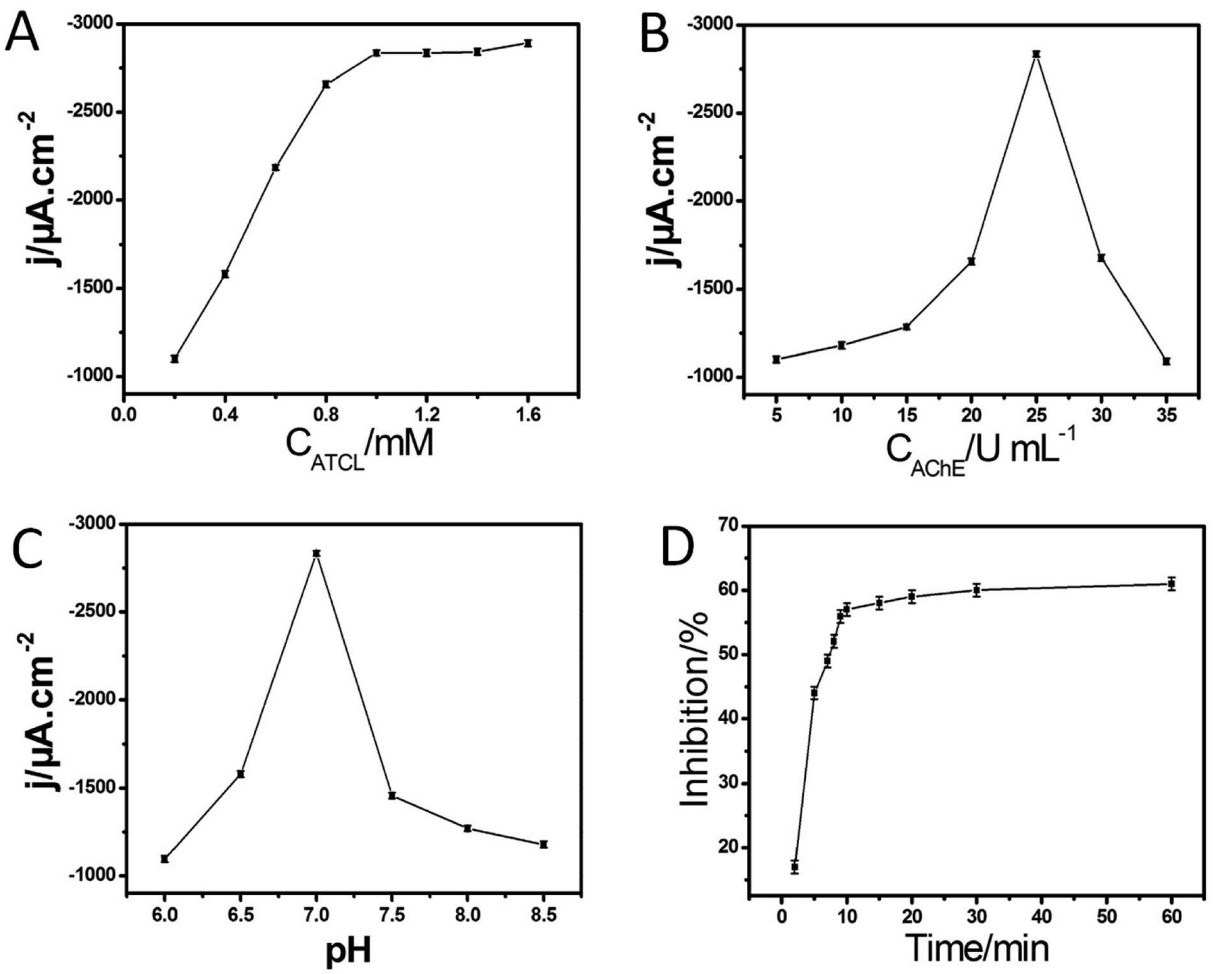


Fig. 3 (A) Relationship between current response and the ATCl concentration in 0.1 M PBS (pH = 7.0). (B) The plot of the amperometric response *versus* AChE concentration of the AChE/Cu-H MOFs/NECFE in 0.1 M PBS (pH = 7.0) containing 1.0 mM ATCl. (C) Influence of the pH value on the current response of AChE/Cu-H MOFs/NECFE to 1.0 mM ATCl. (D) Influence of inhibition time on the percentage of the inhibition of the AChE/Cu-H MOFs/NECFE in 0.1 M PBS (pH = 7.0) containing 1.0 mM ATCl, the trichlorfon for inhibition was 20 ng $mL^{-1}$ (the above experiments were completed on the CHI760E electrochemical workstation).

 

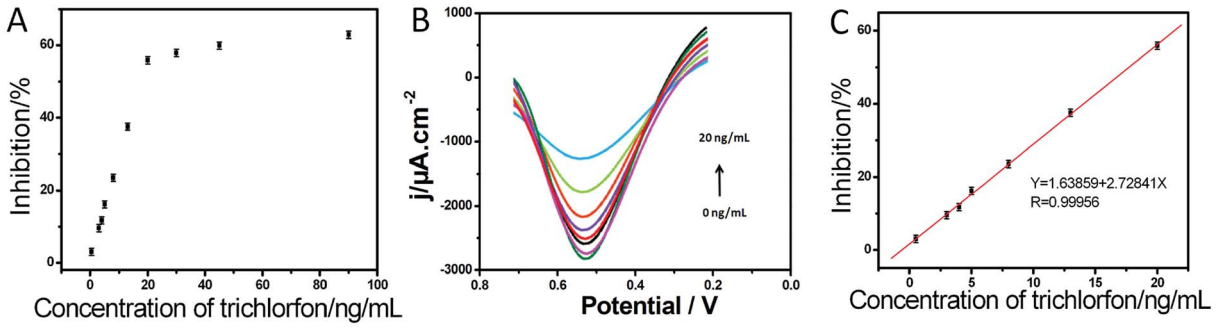


Fig. 4 (A) Inhibition curve of the biosensor with different trichlorfon concentrations (from lower to higher, the inhibitions were corresponding to trichlorfon concentrations of 0.5, 3, 4, 5, 8, 13, 20, 30, 45 and 90 ng $mL^{-1}$, respectively) in 0.1 M PBS (pH = 7.0) containing 1.0 mM ATCl. (B) DPV curves and (C) calibration curve for trichlorfon determination in 0.1 M PBS (pH = 7.0) containing 1.0 mM ATCl.

Fig. 3C, the maximum amperometric response of the AChE/Cu-H MOFs/NECFE to 1.0 mM ATCl was obtained at pH = 7.0, which is in agreement with most of the reported AChE biosensors that exhibited the maximum amperometric response at neutral conditions.[32] The underlying reason for this phenomenon might be that the Cu-H MOFs/NECFE composite was synthesized under neutral conditions; hence, when the composite was in a solution of pH 7, its structure was the most stable. One of the most influencing parameters in pesticide analysis was the incubation time for inhibition. With the increase in incubation period, the percentage of inhibition also increased. The incubation time required for inhibition was checked at different time intervals from 2 to 60 min (Fig. 3D (ESI†)). With an increase in incubation time, inhibition increased and reached the maximum value after the incubation time of 10 min in 20 ng $mL^{-1}$ trichlorfon solution. Thus, 10 min incubation time was used for the assay.

### 3.4 Application of AChE-inhibition biosensors: detection of trichlorfon

Under optimal conditions, the inhibition was proportional to the trichlorfon concentration ranging from 0.25 to 20 ng $mL^{-1}$ (Fig. 4), with the detection limit of 0.082 ng $mL^{-1}$. The performance of this AChE/Cu-H MOFs/NECFE compared with that of other reported AChE biosensors is summarized in Table 1. It showed that the present AChE/Cu-H MOFs/NECFE exhibited comparable or lower detection limit, indicating that Cu-H MOFs/NECF had multiple functions in enzyme immobilization. On one hand, the nitrogen-doped characteristic could maintain the activity of the enzyme; on the other hand, high specific surface area and good electrical conductivity of the compound material could contribute significantly to the sensitivity enhancement.

### 3.5 Precision of measurements, selectivity and stability of biosensor

The inter-assay precision was estimated using five different electrodes for the determinations in 1.0 mM ATCl after being treated with 10 ng $mL^{-1}$ trichlorfon solutions for 10 min. The R.S.D. of inter-assay was found to be 3.9%, indicating acceptable precision and reproducibility. The interferences from the other electroactive phenol derivative (such as nitrophenol, hydroquinone and catechol) and other oxygen-containing inorganic ions ($SO_4^{2-}$, $NO_3^-$, sodium citrate) were

Table 1 Comparison of the performance of various AChE biosensors applied to the detection of pesticides

| Method | Pesticide detected | Linear range | Detection limit | Ref. |
|---|---|---|---|---|
| AChE-(*x*GnPs)-chitosan | Parathion | 0.005–0.039 μM | 0.158 nM | 33 |
| AuNPs-MWCNTs-chitosan | Monocrotophos | 0.1–10 μM | 10 nM | 34 |
| AChE/PAMAMb-Au/CNTs/GCE | Carbofuran | 1.06–19.91 ng $mL^{-1}$ | 0.89 ng $mL^{-1}$ | 35 |
| Nafion/AChE/Chit-PB-MWNTs-HGNs/Au | Carbofuran | 1.11–17.70 ng $mL^{-1}$ | 0.55 | 36 |
| NF/AChE-CS/$SnO_2$NPs-CGR-NF/GCE | Carbofuran | $2.21 \times 10^{-4}$ to $2.21 \times 10^{-2}$ ng $mL^{-1}$ $2.21 \times 10^{-2}$ to 2.21 ng $mL^{-1}$ | $1.11 \times 10^{-4}$ ng $mL^{-1}$ | 37 |
| AChE/$Fe_3O_4$–CH/GCE | Carbofuran | 1.11–19.91 ng $mL^{-1}$ | 0.80 ng $mL^{-1}$ | 38 |
| PPy-AChE-Geltn-Glut/Pt | Carbofuran | 0.025–2, 5–60 ng $mL^{-1}$ | 0.12 ng $mL^{-1}$ | 39 |
| | Paraoxon | 0.1–12.5, 12.5–150 ng $mL^{-1}$ | 1.1 ng $mL^{-1}$ | |
| AChE/e-GON-MWCNTs/GCE | Carbofuran | 0.03–0.81 ng $m^{-1}$ | 0.015 ng $mL^{-1}$ | 40 |
| | Paraoxon | 0.05–1, 1–104 ng $mL^{-1}$ | 0.025 ng $mL^{-1}$ | |
| AChE/CNT-$NH_2$/GCE | Paraoxon | 0.055–0.275 ng $mL^{-1}$, 0.275–8.257 ng $mL^{-1}$ | 0.022 ng $mL^{-1}$ | 41 |
| AChE/ZnO-MWCNTs-sG/GCE | Paraoxon | 0.275–7.156 ng $mL^{-1}$ | $2.752 \times 10^{-4}$ ng $mL^{-1}$ | 42 |
| AChE/SWCNT-Co phthalocyanine/GCE | Paraoxon | 5–50 ng $mL^{-1}$ | 3 ng $mL^{-1}$ | 43 |
| AChE/Au-MWNTs/GCE | Paraoxon | 0.028–1.927 ng $mL^{-1}$ | 0.028 ng $mL^{-1}$ | 44 |
| AChE/Cu-hemin MOFs/NECFE | Trichlorfon | 0.25–20 ng $mL^{-1}$ | 0.082 ng $mL^{-1}$ | This work |

investigated. As shown in Fig. S3 (ESI†), the addition of 2 times the amount of nitrophenol, hydroquinone, catechol, $SO_4^{2-}$, $NO_3^-$ and sodium citrate for the determination of 20 ng $mL^{-1}$ trichlorfon did not cause any significant changes in inhibition behavior. Thus, the electrode was selective and could be applied for the determination of trichlorfon in practical samples. When the enzyme electrode was not in use, it was stored at 4 °C under dry conditions. No significant decrease in the response of ATCl was observed in the first 8 day storage. After a 30 day storage period, the sensor retained 94% of its initial current response (Fig. S4, (ESI†)).

### 3.6 Reactivity and real sample analysis

The reactivation of AChE was another important factor influencing the biosensor performance. AChE, which has been irreversibly inhibited by OPs, could be completely reactivated by using nucleophilic compounds such as pralidoxime chloride (PAM-Cl). PAM-Cl PBS solution at a concentration of 5.0 mM was used for reactivation. After the biosensor was used for trichlorfon inhibition, it was immersed in the PAM-Cl solution. After regeneration for 10 min, the activity of the AChE was totally regenerated. With the reactivation procedure, this biosensor could be repeatedly used for 5 cycles with acceptable reproducibility. To further demonstrate the practicality of the proposed biosensor, the recovery test was studied by adding different amounts of trichlorfon into tomato samples. The results are summarized in Table S1 (ESI†). The recoveries were from 96.9% to 103%. These results indicated that the proposed method was highly accurate, precise and reproducible and could be used for direct analysis of relevant samples.

## 4. Conclusion

In this study, a robust, sensitive and stable biosensor has been constructed based on the AChE-modified Cu-H MOFs/NECF composite, which enabled the detection of trace (0.082 ng $mL^{-1}$) organophosphorous compound, trichlorfon. The use of Cu-H MOFs/NECF significantly improved the performance of the biosensor in three aspects. (1) The synergistic effect of the flower-ball-like Cu-hemin MOFs and netlike NECF, which has large surface area, could firmly immobilize more amount of enzymes. (2) The NECF is robust, which ensures that the integrated electrode would not be easily broken. (3) Cu-H MOFs also have the advantage of fast electron transfer, which can enhance the electrical signal. (4) Moreover, the nitrogen elements derived from hemin and melamine could effectively maintain maximum bioactivity of the immobilized enzyme. Owing to these three important enhancement factors, the resulting biosensor showed extremely high sensitivity and low detection limit. Therefore, this sensor is more suitable for trace detection of OP pesticides residue compared with other AChE biosensors.

## Conflicts of interest

There are no conflicts to declare.

## Acknowledgements

This study was financially supported by National Natural Science Foundation of China (81460594), Natural Science Foundation of Jiangxi Province (20171BAB205092), Excellent Youth Foundation of Jiangxi Scientific Committee (20171BCB23045), Key Research and Development Project of Jiangxi Province (20171BBG70112), Special Research Project of Jiangxi University of Traditional Chinese Medicine (2016ZR002).

## References

1 E. Matsumoto and S. Fujimoto, *Bull. Kagawa Agric. Exp. Stn.*, 2003, **56**, 51–56.
2 H. Chen and J. G. Jiang, *Chemosphere*, 2011, **84**, 664–670.
3 A. T. Guimarães, S. D. A. Hc and W. Boeger, *Ecotoxicol. Environ. Saf.*, 2007, **68**, 57–62.
4 X. H. Li, Z. Xie, H. Min, C. Li, M. Liu, Y. Xian and L. Jin, *Electroanalysis*, 2006, **18**, 2163–2167.
5 H. U. Chandrasekara and A. Pathiratne, *Aquaculture*, 2015, **36**, 144–149.
6 L. Hem, S. Khay, J. H. Choi, E. D. Morgan, A. M. Abd ElAty and J. H. Shim, *Toxicol. Res.*, 2010, **26**, 149–155.
7 S. Suzuki, *Bunseki Kagaku*, 1995, **44**, 41–48.
8 G. M. Wang, H. Dai, Y. G. Li, X. L. Li, J. Z. Zhang, L. Zhang, Y. Y. Fu and Z. G. Li, *Food Addit. Contam., Part A: Chem., Anal., Control, Exposure Risk Assess.*, 2010, **27**, 983–988.
9 D. M. Huang, Y. Q. Cai, H. J. Yu, Y. F. Shi and X. Y. Huang, *Adv. Mater.*, 2012, **554–556**, 1943–1946.
10 W. Wei, S. Dong, G. Huang, Q. Xie and T. Huang, *Sens. Actuators, B*, 2018, **260**, 189–197.
11 R. Montes, F. Céspedes, D. Gabriel and M. Baeza, *J. Nanomater*, 2018, **2018**, 1–13.
12 S. Dong, L. Peng, W. Wei and T. Huang, *ACS Appl. Mater. Interfaces*, 2018, **10**, 1–26.
13 J. C. Dutta and P. K. Sharma, *IEEE Sens. J.*, 2018, **18**, 3090–3097.
14 J. Gong, L. Wang and L. Zhang, *Biosens. Bioelectron.*, 2009, **24**, 2285–2288.
15 S. Sotiropoulou and N. A. Chaniotakis, *Anal. Chim. Acta*, 2005, **530**, 199–204.
16 J. Wang, A. M. Musameh and Y. Lin, *J. Am. Chem. Soc.*, 2003, **125**, 2408–2409.
17 J. W. And and M. Musameh, *Anal. Chem.*, 2003, **75**, 2075–2079.
18 A. I. Gopalan, K. P. Lee, D. Ragupathy, S. H. Lee and J. W. Lee, *Biomaterials*, 2009, **30**, 5999–6005.
19 F. Li, J. Peng, J. Wang, H. Tang, L. Tan, Q. Xie and S. Yao, *Biosens. Bioelectron.*, 2014, **54**, 158–164.
20 D. Du, S. Chen, J. Cai and A. Zhang, *Talanta*, 2008, **74**, 766–772.
21 B. Khalilzadeh, H. N. Charoudeh, N. Shadjou, R. Mohammad-Rezaei, Y. Omidi, K. Velaei, Z. Aliyari and M. R. Rashidi, *Sens. Actuators, B*, 2016, **231**, 561–575.
22 R. Hu, W. Wen, Q. Wang, H. Xiong, X. Zhang, H. Gu and S. Wang, *Biosens. Bioelectron.*, 2014, **53**, 384–389.

23 J. Chen, R. Zhu, J. Huang, M. Zhang, H. Liu, M. Sun, L. Wang and Y. Song, *Analyst*, 2015, **140**, 5578–5584.
24 C. Gong, Y. Shen, J. Chen, Y. Song, S. Chen, Y. Song and L. Wang, *Sens. Actuators, B*, 2017, **239**, 890–897.
25 Y. Song, D. Su, Y. Shen, C. Gong, Y. Song and L. Wang, *Anal. Methods*, 2016, **8**, 4547–4553.
26 Y. Song, J. Chen, H. Liu, Y. Song, F. Xu, H. Tan and L. Wang, *Electrochim. Acta*, 2015, **158**, 56–63.
27 P. Ling, J. Lei, L. Zhang and H. Ju, *Anal. Chem.*, 2015, **87**, 3957–3963.
28 Y. Guo, D. Liu, L. Jing, S. Guo, E. Wang and S. Dong, *ACS Nano*, 2011, **5**, 1282–1290.
29 B. L. Li, H. Q. Luo, J. L. Lei and N. B. Li, *RSC Adv.*, 2014, **4**, 24256–24262.
30 K. Wang, D. Feng, T. F. Liu, J. Su, S. Yuan, Y. P. Chen, M. Bosch, X. Zou and H. C. Zhou, *J. Am. Chem. Soc.*, 2014, **136**, 13983–13986.
31 J. He, H. Yang, Y. Zhang, J. Yu, L. Miao, Y. Song and L. Wang, *Sci. Rep.*, 2016, **6**, 36637.
32 D. V. B. Kandimalla and H. J. Prof, *Chem.–Eur. J.*, 2006, **12**, 1074–1080.
33 A. C. Ion, I. Ion, A. Culetu, D. Gherase, C. A. Moldovan, R. Iosub and A. Dinescu, *Mater. Sci. Eng., C*, 2010, **30**, 817–821.
34 P. Norouzi, M. Pirali-Hamedani, M. R. Ganjali and F. Faridbod, *Int. J. Electrochem. Sci.*, 2010, **5**, 1434–1446.
35 Y. H. Qu, S. Qian, X. Fei, G. Y. Shi and L. T. Jin, *Bioelectrochemistry*, 2010, **77**, 139–144.
36 C. Zhai, X. Sun, W. Zhao, Z. Gong and X. Wang, *Biosens. Bioelectron.*, 2013, **42**, 124–130.
37 Q. Zhou, L. Yang, G. Wang and Y. Yang, *Biosens. Bioelectron.*, 2013, **49**, 25–31.
38 T. Jeyapragasam and R. Saraswathi, *Sens. Actuators, B*, 2014, **191**, 681–687.
39 R. R. Dutta and P. Puzari, *Biosens. Bioelectron.*, 2014, **52**, 166–172.
40 Y. Li, R. Zhao, L. Shi, G. Han and Y. Xiao, *RSC Adv.*, 2017, **7**, 53570–53577.
41 G. Yu, W. Wu, Q. Zhao, X. Wei and Q. Lu, *Biosens. Bioelectron.*, 2015, **68**, 288–294.
42 P. Nayak, B. Anbarasan and S. Ramaprabhu, *J. Phys. Chem. C*, 2013, **117**, 13202–13209.
43 A. N. Ivanov, R. R. Younusov, G. A. Evtugyn, F. Arduini, D. Moscone and G. Palleschi, *Talanta*, 2011, **85**, 216–221.
44 N. Jha and S. Ramaprabhu, *Nanoscale*, 2010, **2**, 806–810.